Trop J Nat Prod Res, January 2021; 5(1):145-164 ISSN 2616-0684 (Print)
ISSN 2616-0692 (Electronic)

Tropical Journal of Natural Product Research

Available online at https://www.tjnpr.org

Original Research Article

The Structure-Based Virtual Screening for Natural Compounds that Bind with the Activating Receptors of Natural Killer Cells

Adekunle B. Rowaiye[1,2], Solomon O. Oni[1]*, Ikemefuna C. Uzochukwu[3], Alex Akpa[1], Charles O. Esimone[2]

[1]*Department of Medical Biotechnology, National Biotechnology Development Agency, Abuja, Nigeria*
[2]*Department of Pharmaceutical Microbiology and Biotechnology, Faculty of Pharmaceutical Sciences, Nnamdi Azikiwe University, Anambra State, Nigeria*
[3]*Department of Pharmaceutical and Medicinal Chemistry, Faculty of Pharmaceutical Sciences, Nnamdi Azikiwe University, Anambra State, Nigeria*

ARTICLE INFO

Article history:
Received 05 October 2020
Revised 07 December 2020
Accepted 22 January 2021
Published online 03 February 2021

ABSTRACT

The natural killer (NK) cells are responsible for immuno-surveillance against cancer and virally -infected cells. Ligand-binding with the activating receptors of the NK cells induces the tyrosine phosphorylation of the Immunoreceptor Tyrosine–based Activation Motif (ITAM) of adaptor proteins and triggers the direct cytotoxicity and the production of inflammatory cytokines through signal pathways. In this study, 1,697 natural compounds were obtained from 79 edible tropical plants through data mining. The *in silico* molecular docking simulations of these compounds were executed against 18 activating NK cell receptor targets using the Python Prescription (PyRx) 0.8 software incorporating both Vina and AutoDock 4.2 plug-in tools. An arbitrary docking score ≥ -7.0 kcal/mol was chosen as cut-off value. Further screening for ligand efficiency, drug-likeness, Absorption Distribution Metabolism Excretion and Toxicity (ADMET) properties, Pan Assay Interference Compounds (PAIN), and possible aggregation behavior were performed. The ligand similarity analysis, phylogenetic analysis of the receptors, and binding site analysis were also performed. The results revealed 17 bioactive and non-promiscuous compounds that have good physicochemical and pharmacokinetic properties. Six of the identified compounds bound to 15 or more receptors with a free energy value ≥ -7.0 kcal/mol.

Keywords: Cytotoxicity, Activating Receptors, Ligands, Cytokines, Immunoreceptor Tyrosine–based Activation Motif.

Introduction

Cancers are a group of diseases characterized by erratic cell growth which invade and spread into other parts of the body.[1,2] They are caused by DNA damage and an ineffective DNA repair mechanism. According to a 2015 WHO report, cancer is the second leading cause of death globally and there were 90.5 million incidences of cancer in 2015 which accounted for 8.8 million deaths.[3]
Cancers are caused by a persistent damage to DNA which culminates into mutations of certain gene sequences in the human genome.[4] Expression of these mutant sequences lead to an autonomous and unregulated hyper-proliferation of cells; insufficient apoptosis; altered differentiation and metabolism; genomic instability; and immortalization.[5] The abnormal proliferation of cells is due to alterations in the cell cycle replication mechanism due to nuclear and cytoplasm distortions. These changes include hyperchromatism, increased telomerase expression, prominent nucleoli, irregular chromatin distribution within nuclei, and increased size of nucleus, pleomorphism, and chromosomal translocations.[6,7]
Available cancer therapies such as chemotherapy are non-selective as other normal rapidly dividing cells (including immune cells) are destroyed. Another major frustration faced by clinicians and researchers includes the evasive nature of cancer cells as they beat the immune system by their molecular 'anonymity'. This is further complicated by their rapid multiplication, invasiveness, and malignant abilities. Through intricate mechanisms, the rapidly dividing aberrant cells are able to evade the immune system, invade the surrounding tissue, enter into the lymph nodes, and metastasize.[8] Therefore, the development of potential therapeutic agents must consider selectivity, specificity, and efficacy.
NK cells are responsible for immune-surveillance of tumor and virally-infected cells. To unlock or lock the cytotoxic potentials of this unique population of immune cells are activating and inhibiting receptors respectively.[9] The immunomodulatory potential of NK cells guarantees that the immune system does not fight against itself. Therefore, NK cell-targeted therapies hold great promise in the treatment of cancers.[9]

*Corresponding author. E mail: goodnessoni@gmail.com
Tel: +234-703-228-3653

Citation: Rowaiye AB, Oni SO, Uzochukwu IC, Akpa A, Esimone CO. The Structure-Based Virtual Screening for Natural Compounds that Bind with the Activating Receptors of Natural Killer Cells. Trop J Nat Prod Res. 2021; 5(1):145-164. doi.org/10.26538/tjnpr/v5i1.21

Official Journal of Natural Product Research Group, Faculty of Pharmacy, University of Benin, Benin City, Nigeria.

Materials and Methods

Materials

The protein and ligand databases used were: Protein Databank, Uniprot, and PubChem. The webservers used were: pkCSM, Clustal Omega, ExPASy, Molinspiration, Protein-Ligand Interaction Profiler (PLIP), SWISS-MODEL, SwissADME, ChemMine, MolProbity, Chiron, and CABS-flex 2.0. The software used are: Discovery studio 2017, Open Babel, PyMOL, and Python prescription (PyRx) 0.8.

Identification of targets

The activating receptors of NK cells were identified by an extensive literature review. Validation of these molecular targets was also by empirical evidence provided by relevant research publications. The 3D crystallographic structures of these proteins were downloaded from the RCSB protein databank in the pdb format and visualized using the PyMOL software.[10] The homology modeling of the proteins whose

structures could not be obtained in the RCSB protein databank was executed using the SWISS-MODEL web-server.[11] The templates of closely related proteins were used for the modeling as seen in Table 1.

Analysis and validation of protein structures

An all-atom structural validation and dihedral-angle diagnostics of the protein crystallography was conducted using the online server, MolProbity and the Ramanchandran plots were also obtained as seen in Table 2.[12]

Preparation of protein targets for docking

In preparing the protein targets for molecular docking, all available water molecules, native ligands, and unwanted chains were removed using the PyMOL software.[10] Energy minimization of the protein targets to resolve steric clashes was done using the online tool, *Chiron* as seen in Table 3.[13] The PyRx software was used to convert the protein targets from pdb to pdbqt files.[14]

Building of library of natural bioactive compounds

A library of 1,697 compounds was built from an extensive data mining from the literature review of 79 plants (See supplementary data) predominantly found in Nigeria and tropical Africa. The 3D structures of these natural compounds were downloaded from the PubChem chemical database in their Spatial Data File (SDF) formats.[15] The properties of these compounds such as molecular weight, canonical SMILES, number of heavy atoms, hydrogen bond donors, hydrogen bond acceptors, Log P, and topological polar surface area were obtained from PubChem.[15]

Preparation for docking

Prior to docking, 1,697 natural compounds were screened for bioavailability using the Lipinski and Veber rules. As stated by Lipinski, the drug-like properties include a MW $\leq$ 500, Hydrogen Bond Donor $\leq$ 5, Hydrogen Bond Acceptor $\leq$ 10, and a Log P value $\leq$ 5. Further screening was done for cellular permeability using the Veber's rule. Only compounds of Topological Polar Surface Area (TPSA) values of $\leq$ 140 Å and number of rotatable bonds $\leq$ 10 were successful.

The docking protocol was validated by using a structure from the Protein Data Bank. The molecule which is the Adhesion Domain of Human CD2 (PDB ID: 1GYA) was downloaded in pdb format and separated from N-Glycan which is the native ligand. The separated molecules were docked together using PyRx 0.8. The docked result was superimposed on the pure protein structure and compared with the original 1GYA structure found in the data bank (Figure 2).

Ligands were uploaded unto PyRx 0.8 through the Open Babel plug-in tool. For stable conformation, the conjugate gradient descent was used as optimization algorithm. The Universal Force Field (UFF) was used as the energy minimization parameter.

The SDF formats of all ligands were converted to the pdbqt format in readiness for docking. The grids were maximized to cover the entire binding site of the ligand. Molecular docking of ligands against protein targets was executed through AutoDock Vina plug-in tool of the PyRx software. Based on the scoring function, the best fits were obtained and saved in excel files.

Screening for potency

The first stage of the screening was for drug potency. Molecular docking was used as the first step in the virtual screening process, and the docking scores were used as empirical predictors of the strength of the intermolecular interactions between the receptors, and the ligands (See supplementary data).

A uniform docking scoring cut-off of -7.0 kcal/mol was used to serve as a general border line for the binding energies obtained between the receptors, and the ligands. Because drug potency is an aggregate of the binding affinity and efficacy, further screening for efficacy was executed by imploring the use of three Ligand Efficiency Metrics (LEM) which are the Ligand Efficiency (LE), ligand-efficiency-dependent lipophilicity, (LELP) and Ligand-lipophilicity efficiency (LLE). The LE was calculated as the binding energy divided by the number of heavy atoms; the LELP is the Log P value of the ligand divided by the LE; and the LLE is the binding energy minus the log P. The cut-offs are $\geq$ 0.3 for LE; -10 to 10 for LELP; and $\geq$ 5.0 for LLE (See supplementary data for results).

Further screening for Oral Bioavailability, Promiscuity and pharmacokinetic properties

After the initial screening for drug-likeness using the Lipinski and Veber rules, the natural compounds were screened for saturation and promiscuity using the SwissADME webserver.[16] Using the canonical SMILES, a Quantitative-Structural Activity Relationship (QSAR) based prediction of the Absorption, Distribution, Metabolism, Excretion, and Toxicity (ADMET) properties of the selected compounds was executed using the pkCSM webserver and this was used for further screening. (See supplementary data for results).

Prediction of bioactivity

Using the Molinspiration webserver, the bioactivity of the compounds was predicted as seen in Table 10.

Specificity/promiscuity analyses

After the initial screenings, the comparative binding affinity analysis of all the protein-ligand interactions was done to check for specific and promiscuous binding (Table 11).

Structural similarity analyses

The similarity analyses of all the screened ligands were done using the *ChemMine* webserver as shown in Table 12.[17] A structural analysis of the protein targets was done through a pairwise Percent Identity Matrix. The results are seen in Table 13. A multiple sequence alignment of the amino acid residues of the extracellular domain of all the receptor targets and subsequently the phylogenetic analysis was done using the Clustal Omega webserver.[18] The results are shown in Figure 1.

Binding site analyses

The poses of the selected ligands as they interact with the receptors during docking were saved on PyRx and viewed on PyMOL. The protein structures were superimposed on PyMOL and saved in the pdb format. The structures were uploaded into the Protein-Ligand Interaction Profiler (PLIP) webserver for the analysis of their binding sites.[19] The summary of all the protein-ligand interactions is shown in supplementary data.

Normal Mode Analysis

The Root Mean Square Fluctuation (RMSF) plots of the amino acid residues of native and mutant (after binding with ligand) proteins were obtained using the CABS-flex 2.0 webserver (Table 14).[20]

Results and Discussion

Preparation for docking

Profiling and homology modeling of the protein structures: From Table 1, the four proteins modeled have very high percentage (between 85.96 and 92.44%) similarity with their templates. Usually, protein structures with over 30% identity to their templates can be predicted with an accuracy equivalent to a low-resolution X-ray structure. [21] In such high sequence identities, the major errors in modeling arise from the use of a poor template and inaccurate alignment of target-template sequence.[22]

Ramachandran Analysis

The Ramachandran plot was used to validate the macromolecular crystal structures of all the receptor targets to be studied by revealing the torsional conformation of their amino acids. From Table 2, all the protein structures have over 80% and 90% of their residues within the favoured and allowed regions respectively signifying good stereochemical quality. None of the proteins are intrinsically-

disordered because of the chemical correctness of the torsional angles of their backbone.[23]
When the φ and ψ angles are combined, an outlier residue has unusual torsional angles. All the protein structures had ramachandran outliers less than 0.05% signifying quality backbone conformation.[24] In this regard, the two proteins of least structural quality are KIR2DS1 and KIR2DS3 with 9 (0.046%) and 7 (0.036%) outliers respectively. These two proteins were homologically modeled from the same template, KIR3DL1. The relatively higher percentage of outliers found in these two proteins may be due to partially disordered large loops in the template. Loops have high electronic densities due to their structural flexibility and randomness and hence their residues show a broader range of dihedral angle values.[25]
Though from Table 2, all the 18 proteins meet the required cut-off, IL15Rα and CD2 have the highest and lowest structural quality respectively. This difference is due to the method used for the structural analysis of these proteins. The structure of IL15Rα (PDB 4gs7) was obtained from x-ray crystallography, while CD2 (PDB1gya) was obtained from solution nuclear magnetic resonance (NMR). NMR gives a lesser resolving power than X-ray crystallography because it offers much more complex information from the same material. Most successful computational protein design use high-resolution X-ray crystallographic structures as templates.[26]

Energy minimization
As two non-bonding atoms in a protein structure approach, an atomic overlap (contact) occurs resulting in Van der Waals repulsion energy greater than 0.3 kcal/mol and subsequently leading to a steric clash. The webserver, Chiron is able to resolve severe steric clashes with minimal perturbation of the backbone of the native structure (less than 1 Å Cα RMSD).
Chiron generates a clash score which is a size-independent parameter obtained mathematically by the ratio of total VDW repulsion energy to the total number of contacts. From data generated from high-resolution structures, Chiron is able to determine if a protein has artifacts (excessive steric clashes) and return the clash score to physiological acceptability (0.02 kcal.mol−1.contact−1).[13]
A reduction in the total van der Waals (VDW) repulsion energy (Kcal/mol) of the clashing atoms would lead to a reduction in the steric clashes and consequently improve ligand-binding This is done computationally by rearranging this collection of non-bonding atoms in such a way that their inter-atomic forces are as close to zero as possible.[13]
From Table 3, all 17 minimized structures have a physiologically acceptable clash ratio (clash score) of less than 0.02. There is no reduction in the total number of clashes and total VDW repulsion energy (Kcal/mol) in NCR1 and IL2Rγc signifying that these proteins already stable conformations. There is also no reduction in the steric clashes in all the protein structures that were modeled which are KIR2DS1, KIR2DS3, KIR2DS5, and NKG2E. This is because the SWISSMODEL webserver during the modeling process repairs distorted geometries or steric clashes through energy minimization. [27] IL2Rβ was not minimized probably due to missing heavy atoms of the backbone.[13]

Validation of docking protocol
1gya consists of CD2 and N-glycan (alpha-d-mannose, beta-d-mannose, and N-acetyl-d-glucosamine) molecules. Figure 2 shows the images of the original 1gya and that of the separated, docked, and superimposed. These two closely resemble thereby validating the docking protocol. [28]

Screening for Bioavailability
Prior to docking, a library of 1,697 compounds was screened for bioavailability using the Lipinski and Veber rules. The predictors of good oral bioavailability include number of rotatable bonds, hydrogen bond acceptors (≤ 10), hydrogen bond donors (≤ 5), molecular weight (≤ 500), low polar surface area (TPSA ≤ 140), and lipophilicity (Log P ≤ 5.0).[29,30] 1,048 front-runner compounds were selected with zero violations to both rules.
One limitation of the Lipinski rule is the fact that it only applies to compounds that are transported by diffusion through cell membranes. Actively transported compounds are exempted from this rule.[31] The conformational features of these compounds closely resemble endogenous metabolites and as such active transport is enhanced through ATP-dependent mechanisms.[32] This explains why so many proven compounds that have elicited *in vitro* cytotoxicity have been screened out.[33]

Screening for potency
Binding Affinities: For the purpose of screening, a uniform docking score of -7.0 kcal/mol was chosen as a cut-off value as this depicts strong protein-ligand binding. The choice of a lower docking score would increase the amount of data to be handled and also affect potency. [34] The binding affinity values reveal the strength of ligand-protein interaction. After docking 1,048 ligands against 18 receptors, 377 front-runner compounds were selected as seen in Table 5 (summary of screening results). This implies that approximately 36% of the screened compounds obtained mainly from fruits, and vegetables have strong binding affinities with the activating receptors of the NK cells. This data further establishes the fact that phytochemicals of fruits, mushrooms, and vegetables modulate NK cell activities and thereby promote the prevention of cancer.[9]
Table 6 shows the summary of distributions and frequencies of receptor-ligand dockings at frequencies ≤-7.0 kcal/mol. NKG2D, NKG2E, and PILR bound with the highest number of ligands in the library. NKG2D is known to be a promiscuous receptor and this suggests why it binds to a high number of ligands in the study. [35] NKG2E which was modeled with a NKG2A template (85.96% similarity) and NKG2D have similar hydrophobicity plots suggesting the possibility of promiscuity. PILR is also known to be a promiscuous type I transmembrane receptor and this suggests why it binds to a high number of ligands in the study.[36]
On the contrary, Table 6 also reveals that NCR2, CD2, NKG2C, IL2Rβ, and IL15Rα have less than 5%. This is suggestive of the fidelity of these receptors as they specifically bind to only a few ligands.[37]
Ligand Efficiency Metrics: LEM screening identifies compounds with greater potency and ADMET properties. [38] Maintaining the potency of a compound with the right molecular size and lipophilicity is a challenge in multi-parameter lead optimization. It is more ideal to optimize hits with the highest ligand efficiencies than those with the strongest binding affinities.[39] Table 5 reveals that a total of 192 front-runner compounds were obtained after screening using the LEM. The screened compounds had a LE of ≥0.3; an LELP of between -10 and 10; and LLE ≥ 5.0.39 Good LE values indicate that compounds have the desired potency at the appropriate weight. With lower molecular weight, there is also room for lead optimization to improve the potency and pharmacokinetic properties.[40]

QSAR-Based ADMET, Saturation and Promiscuity predictions
As seen in Table 5, a total of 69 front runner compounds emerged from the screening for saturation, promiscuity, and pharmacokinetic properties. Many of the eliminated compounds remain viable candidates for lead optimization. Many of the eliminated compounds are also known to have strong antioxidant and immunomodulatory properties.
Molecular complexity which is measured by the carbon bond saturation (fraction of sp^3 carbons - fsp^3) plays a vital role drug discovery. Saturation directly correlates with solubility and saturated hydrocarbons have stability of the chemical bonds which make them unreactive. [41] As seen in Table 8, all compounds with values less than 0.25 are unsaturated and therefore eliminated.
While drug promiscuity may have its advantage, it elicits undesirable side effects due to ligand interactions with multiple protein targets in the biological system. A good predictor of promiscuity in bioassays is aggregation. Most drugs are not promiscuous even at a high concentration. However, some have tendency to self-aggregate in aqueous media. These compounds have disruptive functional groups that can interfere with bioassays by causing activity artifacts leading to

ISSN 2616-0684 (Print)
ISSN 2616-0692 (Electronic)

false positive results. [42] As seen in Table 8, there are no PAIN (Pan-assay Interference) compounds.

The absorption profile of a drug affects its bioavailability and consequently its efficacy and pharmacological effect.[43] Parameters such as water solubility, Caco-2 cell permeability, Human Intestinal Absorption (HIA), and Skin Permeability are within accepted range.[44-47] Permeability glycoprotein (P-glycoprotein or Pgp) is a transporter protein that is located on the cell membrane. It is an ATP-dependent efflux pump which flushes out xenobiotics and toxic substances thereby limiting their cellular absorption.[48] From Table 7, all Pgp inhibitors were eliminated to avoid cellular toxicity. However, Pgp inhibitors can be used in overcoming multidrug resistance in cancers or administered with P-gp substrates to overcome the challenges of poor bioavailability associated with the later.[48]

The distribution of a drug determines the pharmacological effect and duration of action. From Table 7, the predicted distribution parameters such as steady state volume of distribution (VDss), Fraction unbound (Fu), Blood Brain Barrier (BBB) permeability and CNS permeability are within pharmacological range.[49]

Many drugs that affect CYP450 enzymes by either inducing or inhibiting their activities. CY3A4 is the most abundant isoform in the liver. Inhibiting this enzyme can block it and cause an elevation of levels of substrate leading to toxicity or undesirable pharmacological effects.[50,51] From Table 8, all CYP450 enzyme inhibitors were eliminated.

The rate at which a drug is excreted determines the dose. Drug excretion is determined by such parameters as total clearance (CL) which is a total of the renal clearance, hepatic clearance, and the lung clearance. From Table 8, all lead compounds have CL values within accepted pharmacological range. Human Organic Cation Transporter (OCT2) is a renal uptake transporter protein located on the proximal tubule cells. It removes mostly OCT2 substrates which are mostly cationic drugs from the blood into the urine. The concurrent administration of an OCT2 substrate with an OCT2 inhibitor would lead to a toxic intracellular accumulation of the OCT2 substrate.[52] From Table 8, there is no OCT2 substrate.

The toxicity profile of a drug is predicted based on QSAR models such as microbial and fish toxicity, mutagenicity to *Salmonella typhimurium* (Ames Test), Human ether-a-go-go-related gene (hERG) inhibition, skin Sensitization, and hepatotoxicity. All lead compounds were non-mutagens, non-hERG inhibitors and non-dermatoxic. From Table 9, Eugenyl Glucoside, Gibberellin A19, Gibberellin A51, and Gibberellin A53 are predicted to be hepatotoxic. This implies that they possess structural moieties that could elicit the disruption of normal liver function. This kind of hepatotoxicity usually has a predictable dose-response curve. This suggests that doses below the Maximum Tolerated Dose (MTD) cannot induce hepatotoxicity.[53] Other dose-related toxicity indicators which include microbial and fish toxicity, MTD, acute toxicity (LD50), and chronic toxicity are within acceptable pharmacological range. [52]

Bioactivity

Affinity does not necessarily predict activity. Binding ligands could be either agonists or competitive inhibitors. Based on a particular drug target, a compound is considered as active when it's a bioactivity score is more than 0.0; moderately active when score is between −5.0 and 0.0; and inactive when the score is less than −5.0.[54]

Table 10 reveals 17 compounds that are active as nuclear receptor ligands. Many of these compounds are multi-targeted, binding to multiple receptor targets. Bioactivity screening also eliminates promiscuous binding compounds as seen in PILR, NKG2E, and NKG2D receptors.

Specificity-Promiscuity Analyses

There is no correlation between potency and specificity. Selectivity plays a strategic role in drug development. [55] Beyond potency, the selectivity of a drug is also important as this guarantees specificity at the biological target reducing unwanted side effects. [56]

From Table 11, the comparative analysis of binding affinities shows 6 compounds that have absolute binding specificity with a single receptor (NKG2D or NKG2E) at ≤ -7.0 kcal/mol. Specificity also depicts the strength of interaction between ligand and protein. High chemical specificity means that proteins bind to a limited number of ligands. This is important as certain physiological processes might require specificity.[56,57] Compounds such as 4'-Methyl-epigallocatechin, Andrographis Extract, and Gibberellins A17, 19, 29, & 44 have strong binding affinities with 15 and above receptor protein targets.

Similarity analysis

Structural similarity may suggest closeness in biological activity.[58]

Ligand Similarity analyses: As seen in Table 12, a pairwise ligand similarity analyses of Gibberellins A17, A19, A20, A29, A44, A51, and A53 reveal Tanimoto scores ranging from 0.50 to 0.81. Gibberellins A20 and A51 have the same chemical formula but different stereochemistry. Carveol & cis-Carvotanacetol have a Tanimoto score of 0.51. These compounds have been predicted to elicit similar function and would be useful in building pharmacophores for ligand-based drug design.[59]

Receptor similarity: The multi-target binding of the ligands is likely due to the structural similarities of the protein targets. Empirical evidence show that ligands could have the same binding pocket in different proteins.[55] This may be due to genetic similarities of the proteins. Isoforms of the same protein and those that by co-evolution may exhibit similar biochemical reactions might have the same binding sites.[60]

The structural similarity of the target protein was studied using a percent identity matrix in Table 13. Amino acid sequence alignments that produce a pairwise sequence identity >40% is considered high.[61] Out of the 11 members of the Immunoglobulin super family of receptors, KIR2DS1, KIR2DS2, KIR2DS3, KIR2DS4, and KIR2DS5 are highly similar proteins as they have degree of conservation ranging from 86.53-92.65% (Table 13). Of all the 3 lectin-like receptors, consensus sequences only exist between NKG2E & NKG2C with a 90.04% identity. This signifies that these two sets of proteins are isoforms. NKG2E and CD2 have the least identity of 6.36%.

From Figure 1, all the receptors have a common ancestor and have evolutionary relatedness. An original speciation event occurred resulting in three lineages (roots). The tree also depicts the direction of evolution, with the flow of genetic information moving from the roots, through the clades, to the branches, to the taxa, and outgroups. Root 3 consists exclusively of the KIR2DS series of receptors. Root 1 Clade 2 also consists of all the lectin-like receptors. Most closely related pairs exist in the sister taxa. KIR2DS1-5 are the most closely related family in all the 18 receptors. The NCR 1-3 are the most divergent.

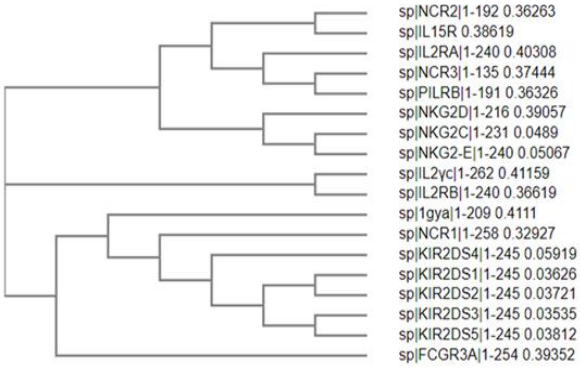

Figure 1: The phylogenetic relationship of the 18 activating NK cell receptors

Binding site analyses

All residues that are involved in the ligand–protein interactions are located within the extracellular domains of the receptor (See supplementary data). Receptor signaling should commence from the extracellular domain through the helical domain to the cytoplasmic

ISSN 2616-0684 (Print)
ISSN 2616-0692 (Electronic)

domain. The greater the number of ligand interactions within the functional domains, the greater the biological activity of the protein is triggered. The 18 receptor targets have functional domains such as Immunoglobulin-like (C and V types), sushi, C- type lectin, and fibronectin type III domains. For example, as seen in supplementary data, Gibberellin A53, 4'-Methyl-epigallocatechin, and Gibberellin A51 have all their interactions (hydrophobic and hydrogen bonds) within the C2 type 1 and C2 type 2 domains of the KIR2DS4 receptor (N.B. A value of 5 should be added to all the residue numbers for KIR2DS4 to take care of the rearrangement during energy minimization).IL2Rβ has 5 binding sites. Proteins with multiple binding sites show cooperativity. The assembly of the IL2R-IL15R complex allows interfaces between these proteins to create hydrophobic pockets for ligand binding. However, the binding at the original site affects the affinity of all the other sites.[62]

Normal Mode Analysis

Protein flexibility is determined by fluctuations of the alpha carbon atoms of the amino acids. This is seen as rearrangements of side chains or changes in the backbone. Ligand binding induces conformational changes in the protein structure.[63] The stability of protein-ligand complexes would impact on protein function. As revealed in Table 14, structures with the lowest global fluctuation are indicative of the most stable protein-ligand complexes. Ligands of these most stable complexes are the most suitable drug candidates for their respective receptors. The highest numbers of interacting residues are seen in NKG2-D, PILR, and NKG2-E which have 32, 26, and 22 residues respectively. The lowest RMSF value is seen in the interaction between IL2Rα and Monocrotalline (0.13), while the highest is between KIR2DS2 and Gibberellin A29 (51.13). The highest number of bonds is seen between PILR and Eugenyl Glucoside (12).

Brief review of successful leads

Andrographis Extract obtained from *Andrographis paniculata* (King of Bitters) has exhibited potent anti-inflammatory and anticancer properties. Its chemo-preventive activity is revealed in the growth suppression of cancer cells by inducing apoptosis and by inhibiting PI3K/AKT, NF-kappa B, and other kinase pathways.[64]

In mice, the ethanol extract of *Andrographis paniculata* also significantly induced antibody production and delayed type hypersensitivity response to sheep red blood cells. Regarding non-specific immune response, the Andrographis extract induced significant immunostimulation as measured by proliferation of splenic lymphocytes, thymocytes, and bone marrow cells; the migration of macrophages; and phagocytic activity.[65]

Andrographis paniculata extract is known to be one of the natural products that enhance the efficiency of NK cells in the control of cancer. It promotes NK cell mediated lysis of metastatic tumor cells in mice through an antibody-dependent complement-mediated cytotoxicity.[66] It also significantly increases the production of interleukin-2 and interferon-gamma and decreases pro-inflammatory cytokines such as TNF-α, GM-CSF, IL-1ß, and IL-6 in tumour-bearing animals.[67]

The Gibberellins A17, A19, A20, A29, A44, A51 & A53: Gibberellins (GAs) are a group of closely related plant hormones that regulate several physiological and developmental processes which include germination, elongation, flowering, and fruiting.[68] Gibberellins can be obtained from *Abelmoschus esculentus* (Okra) and *Pisum sativum* (Green peas).[69,70]

Gibberellin has been implicated as a modulator of the plant innate immunity. It plays significant role in plant-microbe interaction, especially as it has to do with the root's basal defense. Successful fungal colonization is due to altering gibberellin signaling in plants.[71] Gibberellin modulates plant immune system by regulating the Salicylic acid (SA), Jasmonic acid (JA), and Ethylene (ET) signaling systems.[72]

There were no direct cytotoxic effects of Gibberellins A17, A19, A20, A29, A44, A51, & A53 found in literature. However, Gibberellin derivatives such as GA-13315 reveal strong anti-neoplastic effects both *in vitro* and *in vivo*. It inhibits the growth and also accelerates the apoptosis of KB oral cancer cells. GA-13315 also possesses anti-angiogenic properties.[73,74]

GA-13315 inhibits the P-glycoprotein thereby reducing multidrug resistance induced by cancer cells and it also triggers the multidrug resistance-associated Protein-1.[75] Other synthesized gibberellin derivatives bearing two alpha, beta-unsaturated ketone units showed strong activity in MTT assay against A549, HepG2, HT29, and MKN28 human cancer cell lines. They also exhibited inhibition to topoisomerase I activity.[76]

Gibberellin A4 is known to be a native ligand to the Fab fragment of the haptenic mouse monoclonal antibody, 4-B8(8)/E9. X ray crystallography of the Fab fragment reveals a typical beta barrel fold which is a common motif of all immunoglobulins.[77] This suggests why Gibberellins might be able to bind to Immunoglobulin-like receptors which have immunoglobulin domains.

4'-Methyl-epigallocatechin: This compound can be found in Locust beans (*Parkia biglobosa*). Epigallocatechin which is found in Green Tea (*Camellia sinensis*) can also be methylated into 4'-Methyl-epigallocatechin found in the human body.[78,79]

Another epigallocatechin derivative, such as epigallocatechin gallate (EGCG) which is also found in Green Tea has anticancer effects. Through cell mediated immunity, EGCG reverses myeloid-derived suppressor cell activity.[80,81]. ECCG is also able to modulate both the innate and adaptive immune systems. In ameliorating experimental arthritis in mice, it upregulates the Nrf-2 antioxidant pathway, induces Indoleamine-2, 3-dioxygenase (IDO)-producing dendritic cells, and increases Treg population.[82]

Shikimic Acid is a cyclohexanecarboxylic acid, obtained from Apples (*Malus domestica*). It exhibits anti-inflammatory and antioxidant activities.[83,84] Shikimic acid complex of platinum (II) is active against Leukemia (L1210 and P388) and B16 Melanoma cell lines.[85] The shikimic acid-based synthesis of zeylenone is widely used as a preparation for chemotherapy in cancer patients.[86] Shikimic acid analogue skeleton is a constituent of several antitumor products.[87]

Table 1: Homology modeling of the proteins

S/N	Receptor name	Uniprot code	Template	% Similarity with template
1.	Killer cell immunoglobulin-like receptor 2DS1	Q14954	KIR3DL1	92.44
2.	Killer cell immunoglobulin-like receptor 2DS3	Q14952	KIR3DL1	88.36
3.	Killer cell immunoglobulin-like receptor 2DS5	Q14953	KIR2DL1	91.96
4.	NKG2-E type II Integral membrane protein	Q07444	NKG2A	85.96

ISSN 2616-0684 (Print)
ISSN 2616-0692 (Electronic)

Table 2: Ramanchandran Plot Analysis of Protein Structures

S/N	Receptor	Favoured Region (98%)	Allowed Region (>99.8%)	No of Outliers (%)	Outlier Residues
1	CD2	81.6% (84/103)	96.1% (99/103)	4 (0.039)	8 GLU (-57.8, 91.6)
					27 SER (-167.0, -50.7)
					52 GLU (-177.9, 85.5)
					72 HIS (61.8, 110.6)
2	NCR2	94.3 (100/106)	98.1(104/106)	2 (0.019)	59 TRP (-73.2, -140.7)
					60 THR (97.5, 67.6)
3	KIR2DS2	95.3% (182/191)	97.9% (187/191)	4 (0.021)	57 ASP (-66.3, 48.6)
					67 GLY (-29.0, 164.6)
					68 PRO (-33.4, 118.0)
					114 PRO (-61.5, -70.2)
4	NCR1	94.1% (175/186)	98.9% (184/186)	2 (0.011)	100 TYR (60.2, -94.5)
					150 VAL (69.5, -34.2)
5	IL2Rα	86.3% (101/117)	96.6% (113/117)	4 (0.034)	22 GLU (-46.7, 99.6)
					112 ASN (-37.9, -169.8)
					116 GLU (150.2, -165.2)
					151 HIS (32.9, 78.8)
6	NKG2C	82.0% (50/61)	96.7% (59/61)	2 (0.033)	4 VAL (34.2, 31.5)
					33 LEU (46.3, 87.5)
7	KIR2DS4	90.2% (174/193)	98.4% (190/193)	3 (0.016)	14 PRO (-64.1, -53.5)
					52 ILE (-91.4, 46.7)
					83 VAL (-118.9, -41.0)
8	NCR3	87.3% (96/110)	100.0% (110/110)	0	
9	IL2Rβ	95.3% (183/192)	100.0% (192/192)	0	
10	γc	94.3% (181/192)	100.0% (192/192)	0	
11	IL15Rα	96.9% (63/65)	100.0% (65/65)	0	
12	PILR	94.1% (222/236)	97.9% (231/236)	5 (0.021)	A 2 LEU (-58.8, 30.2)
					A 36 ASN (15.7, 74.4)
					A 61 LYS (-25.5, -53.3)
					B 36 ASN (18.0, 77.2)
					B 61 LYS (-22.2, -59.2)
13	NKG2D	93.1% (229/246)	98.4% (242/246)	4 (0.016)	A 116 GLU (-45.4, 83.0)
					B 132 ALA (172.7, 134.5)
					B 164 GLY (-53.6, 56.7)
					B 176 PRO (-31.6, -74.6)
14	CD16	92.7% (140/151)	100.0% (151/151)	0	
15	KIR2DS1	87.3% (172/197)	95.4% (188/197)	9 (0.046)	65 MET (-52.7, -74.3)
					78 ASP (-22.6, 112.8)
					88 SER (-48.2, 176.4)
					89 ARG (-22.7, 102.0)
					105 THR (-22.4, -53.6)
					107 SER (179.3, 55.2)
					135 PRO (-44.3, -50.9)

ISSN 2616-0684 (Print)
ISSN 2616-0692 (Electronic)

					163 GLU (-27.7, 101.6)
					166 ALA (-5.7, -67.1)
16	KIR2DS3	85.8% (169/197)	96.4% (190/197)	7(0.036)	65 THR (-46.5, -75.6)
					78 ASP (-21.0, 113.3)
					89 ARG (-24.8, 104.3)
					107 SER (173.0, 54.7)
					135 PRO (-42.6, -53.0)
					163 GLU (-25.1, 99.9)
					166 ALA (-3.2, -70.1)
17	KIR2DS5	92.2% (178/193)	98.4% (190/193)	3 (0.016)	105 THR (86.7, -37.8)
					188 ASP (92.4, -161.9)
					193 GLY (-56.8, -99.7)
18	NKG2E	86.7% (98/113)	99.1% (112/113)	1(0.009)	149 ASN (61.8, -81.9)

Table 3: Energy Minimization of Protein Structures

S/N	Protein	Structure	Total No. of residues	Total No. of contacts	Total No. of clashes	Total VDW repulsion energy (Kcal/mol)	Clash ratio
1	CD2	Initial	105	1706	131	135.4	0.079
		Final	105	1326	38	21.44	0.016
2	NCR2	Initial	108	1539	55	39.48	0.026
		Final	108	1497	37	26.14	0.017
3	KIR2DS2	Initial	193	2461	79	56.15	0.023
		Final	193	2324	56	35.85	0.015
4	NCR1	Initial	188	2714	84	53.82	0.02
		Final	188	2714	84	53.82	0.02
5	IL2Rα	Initial	123	1520	65	52.26	0.034
		Final	123	1378	39	24.39	0.018
6	NKG2C	Initial	63	788	51	54.34	0.07
		Final	63	701	14	11.35	0.016
7	KIR2DS4	Initial	195	2637	103	85.66	0.032
		Final	195	2398	69	42.26	0.018
8	NCR3	Initial	112	1450	53	38.42	0.026
		Final	112	1394	41	22.95	0.016
9	IL2Rβ	Initial					
		Final					
10	γc	Initial	193	2732	67	39.86	0.015
		Final	193	2732	67	39.86	0.015
11	IL15Rα	Initial	67	847	25	17	0.02
		Final	67	843	25	16.22	0.019
12	PILR	Initial	240	3324	101	66.67	0.02
		Final	240	3402	93	57.85	0.017
13	NKG2D	Initial	250	4424	121	84.66	0.02
		Final	250	4041	115	71.66	0.018
14	CD16	Initial	157	2058	97	79	0.038
		Final	157	2002	54	35.25	0.018
15	KIR2DS1	Initial	199	2507	65	37.54	0.015

ISSN 2616-0684 (Print)
ISSN 2616-0692 (Electronic)

		Final	199	2507	65	37.54	0.015
16	KIR2DS3	Initial	199	2452	73	39.33	0.016
		Final	199	2452	73	39.33	0.016
17	KIR2DS5	Initial	195	2281	55	28.65	0.013
		Final	195	2281	55	28.65	0.013
18	NKG2E	Initial	115	1459	27	16.99	0.012
		Final	115	1459	27	16.99	0.012

Table 4: Lead compounds' compliance with Lipinski & Veber rules

	Pubchem ID	**MW(g/mol)**	**Log P**	**HBD**	**HBA**	**TPS(A^2)**	**No of Rotatable bonds**
4'-Methyl-epigallocatechin	176920	320.29	0.3	5	7	120	2
Andrographis Extract	6436016	350.4	2.2	3	5	87	3
Betulalbuside A	14484636	332.39	-0.3	5	7	120	8
Bisabolone Oxide A	91700388	236.35	2.5	0	2	26.3	1
Carveol	7438	152.23	2.1	1	1	20.2	1
cis-Carvotanacetol	12233170	154.25	2.1	1	1	20.2	1
Eugenyl Glucoside	3084296	326.34	0	4	7	109	6
Gibberellin A17	5460657	378.4	0.8	4	7	132	3
Gibberellin A19	5460209	362.4	0.7	3	6	112	3
Gibberellin A20	5280481	332.4	1.2	2	5	83.8	1
Gibberellin A29	5460028	348.4	0.2	3	6	104	1
Gibberellin A44	5460372	346.4	1.6	2	5	83.8	1
Gibberellin A51	443458	332.4	1.7	2	5	83.8	1
Gibberellin A53	440914	348.4	2.2	3	5	94.8	2
Monocrotalline	9415	325.36	-0.7	2	7	96.3	0
Phellandrenol	76373091	152.23	2	1	1	20.2	2
Shikimic Acid	8742	174.15	-1.7	4	5	98	1

Table 5: Summary of screening results

Total Library of compounds	1697
Bioavailability screening	1048
Docking results cut off	377
Ligand Efficiency Metrics screening	192
Promiscuity and Pharmacokinetics screening	69
Bioactivity screening	17

ISSN 2616-0684 (Print)
ISSN 2616-0692 (Electronic)

Table 6: Summary of distributions and frequencies of receptor - ligand dockings (≤ -7.0kcal/mol)

S/N	Receptor	No. of compounds that exceed cut-off	Total No. of docked compounds	Percentage
1	KIR2DS1	75	1048	7.16
2	KIR2DS2	94	1048	8.97
3	KIR2DS3	80	1048	7.63
4	KIR2DS4	84	1048	8.02
5	KIR2DS5	64	1048	6.11
6	NCR1	58	1048	5.53
7	NCR2	13	1048	1.24
8	NCR3	86	1048	8.21
9	PILR	151	1048	14.41
10	CD16A	74	1048	7.06
11	CD2	25	1048	2.39
12	NKG2C	20	1048	1.91
13	NKG2D	235	1048	22.42
14	NKG2E	161	1048	15.36
15	IL2Rα	100	1048	9.54
16	IL2Rβ	36	1048	3.44
17	γc	55	1048	5.25
18	IL15Rα	26	1048	2.48

Table 7: Absorption and Distribution profile of lead compounds

Ligand	H_20 Solubility	Caco2 perm.	HIA	Skin Perm	P-gp sub.	P-gp I Inb.	P-gp II Inb.	VDss	Fraction unbound	BBB perm	CNS perm
4'-Methyl-epigallocatechin	-3.09	-0.12	60.73	-2.74	Yes	No	No	1.64	0.26	-0.93	-3.27
Andrographis Extract	-3.49	1.07	95.36	-3.79	No	No	No	-0.29	0.28	-0.6	-2.69
Betulalbuside A	-1.94	-0.14	43.96	-3.03	No	No	No	-0.26	0.65	-1.01	-3.65
Bisabolone Oxide A	-3.63	1.62	96.47	-2.52	No	No	No	0.34	0.43	0.55	-3.05
Carveol	-1.78	1.4	95.18	-2.08	No	No	No	0.17	0.55	0.56	-2.58
cis-Carvotanacetol	-2.15	1.37	95.17	-1.93	No	No	No	0.13	0.47	0.58	-2.12
Eugenyl Glucoside	-1.89	0.58	45.71	-2.87	Yes	No	No	-0.38	0.41	-0.99	-3.73
Gibberellin A17	-2.89	0.82	33.03	-2.74	No	No	No	-0.89	0.42	-0.77	-3.31
Gibberellin A19	-2.81	0.96	47.5	-2.74	No	No	No	-1.6	0.42	-0.68	-3.16
Gibberellin A20	-2.64	1.19	98.91	-2.74	No	No	No	-0.83	0.42	-0.21	-3
Gibberellin A29	-2.66	0.69	71.42	-2.74	No	No	No	-0.82	0.47	-0.6	-3.11

ISSN 2616-0684 (Print)
ISSN 2616-0692 (Electronic)

Gibberellin A44	-2.84	1.18	99.3	-2.74	No	No	No	-1.11	0.3	-0.18	-2.29
Gibberellin A51	-2.73	1.14	100	-2.74	No	No	No	-0.97	0.29	-0.09	-2.41
Gibberellin A53	-2.82	0.93	53.27	-2.74	No	No	No	-1.6	0.36	-0.56	-2.31
Monocrotaline	-3.06	0.51	64.76	-3.01	Yes	No	No	0.47	0.74	-0.61	-3.1
Phellandrenol	-1.96	1.49	94.99	-2.33	Yes	No	No	0.22	0.56	0.55	-2.69
Shikimic Acid	-0.52	-0.23	46.68	-2.74	No	No	No	-0.62	0.8	-0.68	-3.58

HIA = Human Intestinal Absorption. Skin Perm = Skin Permeability. P-gp = Plasma glycoprotein. VDSS = Volume of Distribution steady State. BBB = Blood Brain Barrier

Table 8: Metabolism, Excretion, and Saturation and Agglutination profile of lead compounds

Ligand	**CYP2D 6 sub**	**CYP3A4 sub**	**CYP1A 2 inh**	**CYP2C1 9 inh**	**CYP2C 9 inh**	**CYP2D6 inh**	**CYP3A 4 inh**	**Total Clearanc e**	**Rena l OCT 2 sub**	**Fractio n Csp3**	**PAINS #alerts**
4'-Methyl-epigallocatechin	No	No	No	No	No	No	No	0.35	No	0.25	0
Andrographis Extrac t	NO	Yes	No	No	No	No	No	1.18	No	0.75	0
Betulalbuside A	No	No	No	No	No	No	No	1.69	No	0.75	0
Bisabolone Oxide A	No	No	No	No	No	No	No	1.13	No	0.8	0
Carveol	No	No	No	No	No	No	No	0.23	No	0.6	0
cis-Carvotanacetol	No	No	No	No	No	No	No	0.19	No	0.8	0
Eugenyl Glucoside	No	No	No	No	No	No	No	0.26	No	0.5	0
Gibberellin A17	No	No	No	No	No	No	No	0.39	No	0.75	0
Gibberellin A19	NO	Yes	No	No	No	No	No	0.47	No	0.75	0
Gibberellin A20	No	Yes	No	No	No	No	No	0.42	No	0.79	0
Gibberellin A29	No	Yes	No	No	No	No	No	0.42	No	0.79	0
Gibberellin A44	No	Yes	No	No	No	No	No	0.36	No	0.8	0
Gibberellin A51	No	Yes	No	No	No	No	No	0.42	No	0.79	0
Gibberellin A53	No	Yes	No	No	No	No	No	0.43	No	0.8	0
Monocrotaline	No	No	No	No	No	No	No	0.73	No	0.75	0
Phellandrenol	No	No	No	No	No	No	No	0.29	No	0.6	0

ISSN 2616-0684 (Print)
ISSN 2616-0692 (Electronic)

Shikimic Acid	No	No	No	No	No	No	No	0.69	No	0.57	0

Renal OCT2 = Renal Organic Cation transporter

ISSN 2616-0684 (Print)
ISSN 2616-0692 (Electronic)

Table 9: Toxicity profile of lead compounds

Ligand	AMES toxicity	Max. tolerated dose	hERG I inh	hERG II inh	Oral Rat Acute Toxicity (LD_{50})	Oral Rat Chronic Toxicity (LOAEL)	Hepatotoxicity	Skin Sensitisation	*T. Pyriformis* toxicity	Minnw toxicity
4'-Methyl-epigallocatechin	No	0.37	No	NO	2.29	2.93	No	No	0.3	3.75
Andrographis Extract	No	0.13	No	No	2.16	1	No	No	0.49	1.37
Betulalbuside A	No	1.37	No	NO	1.71	3.2	No	No	0.29	3.66
Bisabolone Oxide A	No	0.35	No	No	1.99	1.86	No	Yes	0.73	1.07
Carveol	No	0.84	No	No	1.96	1.89	No	Yes	0.2	1.67
cis-Carvotanacetol	No	0.82	No	No	1.98	1.99	No	Yes	0.32	1.36
Eugenyl Glucoside	No	0.86	No	No	1.95	3.46	Yes	No	0.29	3.8
Gibberellin A17	No	0.44	No	No	2.48	2.7	No	No	0.29	3.1
Gibberellin A19	No	0.4	No	No	2.21	2.28	Yes	No	0.29	2.49
Gibberellin A20	No	0.37	No	No	2.05	2.14	No	No	0.29	1.96
Gibberellin A29	No	0.26	No	NO	2.1	2.5	No	No	0.29	2.69
Gibberellin A44	No	0.15	No	NO	2.06	1.96	No	No	0.29	1.76
Gibberellin A51	No	-0.14	No	NO	2.1	2.36	Yes	No	0.29	1.16
Gibberellin A53	No	0.36	No	No	2.2	2.17	Yes	No	0.29	1.76
Monocrotaline	No	0.42	No	No	2.4	1.99	No	No	0.29	3.88
Phellandrenol	No	0.87	No	No	1.83	1.81	No	Yes	0.09	1.72
Shikimic Acid	No	0.99	No	No	1.16	2.96	No	No	0.26	4.05

hERG = human Ether-a-go-go-related Gene.

ISSN 2616-0684 (Print)
ISSN 2616-0692 (Electronic)

Table 10: Bioactivity profile of front-runner compounds

	Ligand	GPCR ligand	Ion channel mod.	*Kinase Inh.*	Nuclear Receptor Ligand	Protease Inh.	Enzyme Inh	No of Recep. Targets (≤ -7.0 kcal/mol)
1	Andrographis Extract	0.32	0.17	-0.01	0.94	0.26	0.81	16
2	Gibberellin A53	0.39	0.17	-0.35	0.76	0.18	0.42	6
3	Gibberellin A19	0.32	0.10	-0.30	0.69	0.30	0.43	15
4	Gibberellin A51	0.17	0.21	-0.31	0.67	0.16	0.38	14
5	Gibberellin A44	0.34	0.16	-0.21	0.66	0.19	0.36	16
6	Gibberellin A17	0.36	0.11	-0.25	0.63	0.18	0.33	17
7	Gibberellin A29	0.24	0.20	-0.24	0.60	0.19	0.42	15
8	Gibberellin A20	0.22	0.23	-0.21	0.49	0.09	0.30	7
9	4'-Methyl-epigallocatechin	0.37	0.07	0.11	0.48	0.23	0.39	17
10	Monocrotaline	0.36	0.38	-0.05	0.47	0.50	0.28	7
11	Betulalbuside A	0.27	0.35	-0.05	0.38	0.22	0.73	1
12	Carveol	-0.55	0.14	-1.40	0.25	-0.89	0.23	1
13	Bisabolone Oxide A	-0.11	0.10	-0.97	0.24	-0.35	0.56	1
14	Phellandrenol	-0.75	-0.34	-1.07	0.12	-1.14	0.23	1
15	Eugenyl Glucoside	0.05	-0.03	-0.21	0.02	-0.11	0.32	2
16	Shikimic Acid	-0.38	0.22	-1.13	0.01	-0.37	0.65	1
17	cis-Carvotanacetol	-0.50	0.09	-1.09	0.01	-0.62	0.18	1

Table 11: Binding affinities of front runner compounds (post-screening) with cut off value of ≤ -7.0 kcal/mol

S/N	Compounds	Immunoglobulin-like receptors											Lectin-like Receptors			Others			
		KIR2DS1	KIR2DS2	KIR2DS3	KIR2DS4	KIR2DS5	NCR1	NCR2	NCR3	PILR	CD16A	CD2	NKG2C	NKG2D	NKG2E	IL2Rα	IL2Rβ	γc	IL15Rα	# of targets
1	4'-Methyl-epigallocatechin	7.1	8.2	7.0	8.1	7.0	8.4	7.5	8.1	7.2	8.0	7.0	*	7.2	8.8	8.9	7.2	8.3	7.6	17
2	Gibberellin A17	8.9	8.3	8.9	9.0	8.6	8.4		8.6	8.8	7.6	7.7	7.3	8.8	7.4	7.7	7.3	7.4	7.1	17
3	Andrographis Extract	8.0	7.1	7.9	7.4	7.6	7.4	*	7.2	8.3	7.7	7.0	7.2	7.4	7.2	7.2	*	7.	7.2	16

ISSN 2616-0684 (Print)
ISSN 2616-0692 (Electronic)

4	Gibberellin A44	8.2	8.4	8.2	8.2	8.1	8.0	*	8.2	8.3	8.0	7.2	7.0	8.0	*	7.3	7.3	7.7.4	7.0	16
5	Gibberellin A19	8.3	7.5	8.3	8.1	8.3	8.3	*	8.3	8.5	7.4	7.4	7.2	8.4	7.1	7.4	*	7.3	*	15
6	Gibberellin A29	8.2	7.9	8.1	7.7	7.5	7.7	*	8.5	8.7	8.7	7.2	*	7.8	7.7	7.3	7.3	7.6	*	15
7	Gibberellin A51	7.8	8.1	8.0	8.1	7.8	7.5	*	8.5	8.6	8.1	*	7.6	7.7	7.4	7.0	*	7.2	*	14
8	Gibberellin A20	7.4	7.1	7.4	7.0	*	*	*	7.5	7.6	8.2	*	*	*	*	*	*	*	*	7
9	Monocrotaline	7.0	7.3	7.1	*	*	*	*	*	7.5	7.0	*	*	7.1	*	7.0	*	*	*	7
10	Gibberellin A53	*	7.1	*	7.4	7.0	*	*	7.1	7.4	7.2	*	*	*	*	*	*	*	*	6
11	Eugenyl Glucoside	*	*	*	*	*	*	*	*	7.0	*	*	*	*	7.7	*	*	*	*	2
12	Betulalbuside A	*	*	*	*	*	*	*	*	*	*	*	*	*	7.6	*	*	*	*	1
13	Bisabolone Oxide A	*	*	*	*	*	*	*	*	*	*	*	*	*	8.1	*	*	*	*	1
14	Carveol	*	*	*	*	*	*	*	*	*	*	*	*	7.6	*	*	*	*	*	1
15	cis-Carvotanacetol	*	*	*	*	*	*	*	*	*	*	*	*	7.5	*	*	*	*	*	1
16	Phellandrenol	*	*	*	*	*	*	*	*	*	*	*	*	7.8	*	*	*	*	*	1
17	Shikimic Acid	*	*	*	*	*	*	*	*	*	*	*	*	*	7.0	*	*	*	*	1
		9	**10**	**9**	**9**	**8**	**7**	**1**	**9**	**11**	**10**	**6**	**5**	**11**	**10**	**8**	**4**	**7**	**4**	

All binding affinity values are negative.

Table 12: Pairwise Ligand Similarity Analysis of active compounds Using Tanimoto Coefficient

		1	**2**	**3**	**4**	**5**	**6**	**7**	**8**	**9**	**10**	**11**	**12**	**13**	**14**	**15**	**16**	**17**
4'-Methyl-epigallocatechin	1	1.00	0.13	0.14	0.07	0.06	0.07	0.25	0.09	0.11	0.09	0.11	0.08	0.11	0.09	0.14	0.10	0.13
Andrographis Extract	**2**	0.13	1.00	0.22	0.22	0.15	0.12	0.18	0.27	0.28	0.27	0.27	0.29	0.28	0.30	0.22	0.09	0.09
Betulalbuside A	**3**	0.14	0.22	1.00	0.12	0.07	0.10	0.37	0.13	0.14	0.16	0.17	0.15	0.16	0.14	0.17	0.11	0.13
Bisabolone Oxide A	**4**	0.07	0.22	0.12	1.00	0.14	0.19	0.19	0.15	0.19	0.21	0.18	0.19	0.19	0.21	0.22	0.16	0.07

ISSN 2616-0684 (Print)
ISSN 2616-0692 (Electronic)

Carveol	**5**	0.06	0.15	0.07	0.14	1.00	0.51	0.05	0.07	0.08	0.08	0.08	0.08	0.09	0.09	0.08	0.24	0.14
cis-Carvotanacetol	**6**	0.07	0.12	0.10	0.19	0.51	1.00	0.06	0.06	0.08	0.07	0.07	0.06	0.07	0.09	0.09	0.09	0.09
Eugenyl Glucoside	**7**	0.25	0.18	0.37	0.19	0.05	0.06	1.00	0.08	0.09	0.10	0.12	0.10	0.12	0.08	0.16	0.09	0.13
Gibberellin A17	**8**	0.09	0.27	0.13	0.15	0.07	0.06	0.08	1.00	0.80	0.67	0.60	0.66	0.50	0.75	0.21	0.05	0.09
Gibberellin A19	**9**	0.11	0.28	0.14	0.19	0.08	0.08	0.09	0.80	1.00	0.71	0.63	0.70	0.52	0.80	0.24	0.09	0.10
Gibberellin A20	**10**	0.09	0.27	0.16	0.21	0.08	0.07	0.10	0.67	0.71	1.00	0.79	0.81	0.67	0.75	0.26	0.06	0.10
Gibberellin A29	**11**	0.11	0.27	0.17	0.18	0.08	0.07	0.12	0.60	0.63	0.79	1.00	0.68	0.80	0.67	0.27	0.06	0.11
Gibberellin A44	**12**	0.08	0.29	0.15	0.19	0.08	0.06	0.10	0.66	0.70	0.81	0.68	1.00	0.60	0.74	0.25	0.05	0.10
Gibberellin A51	**13**	0.11	0.28	0.16	0.19	0.09	0.07	0.12	0.50	0.52	0.67	0.80	0.60	1.00	0.55	0.29	0.06	0.10
Gibberellin A53	**14**	0.09	0.30	0.14	0.21	0.09	0.09	0.08	0.75	0.80	0.75	0.67	0.74	0.55	1.00	0.23	0.06	0.10
Monocrotaline	**15**	0.14	0.22	0.17	0.22	0.08	0.09	0.16	0.21	0.24	0.26	0.27	0.25	0.29	0.23	1.00	0.09	0.11
Phellandrenol	**16**	0.10	0.09	0.11	0.16	0.24	0.09	0.09	0.05	0.09	0.06	0.06	0.05	0.06	0.06	0.09	1.00	0.15
Shikimic Acid	**17**	0.13	0.09	0.13	0.07	0.14	0.09	0.13	0.09	0.10	0.10	0.11	0.10	0.10	0.10	0.11	0.15	1.00

Table 13: Percent Identity Matrix of Protein Target

		1	**2**	**3**	**4**	**5**	**6**	**7**	**8**	**9**	**10**	**11**	**12**	**13**	**14**	**15**	**16**	**17**	**18**
NCR2	**1**	100	25.12	15.56	15.38	21.69	12.79	10.26	15.19	17.24	21.57	10.85	17.69	14.29	12.82	12.82	12.82	11.97	11.97
IL15Rα	**2**	25.12	100	15.2	14.09	17.13	14.52	19.64	21.05	10.59	14.65	10.45	13.48	15.13	13.73	13.73	13.73	14.38	13.73
IL2Rα	**3**	15.56	15.2	100	21.08	17.91	11.29	11.27	11.27	13.79	18.09	8.46	9.76	6.57	8.45	7.75	9.15	8.45	8.45

ISSN 2616-0684 (Print)
ISSN 2616-0692 (Electronic)

NCR3	**4**	15.38	14.09	21.08	100	26.23	12.16	12.5	12.33	13.57	12.86	9.62	11.58	10.28	12.38	13.33	13.33	15.24	13.33
PILRB	**5**	21.69	17.13	17.91	26.23	100	16.95	12.07	12.07	13.53	12.5	10.16	11.81	12.59	10.42	13.19	11.11	11.81	11.81
NKG2D	**6**	12.79	14.52	11.29	12.16	16.95	100	22.06	22.33	15	15.12	13.21	10.58	13.6	11.11	10.1	11.11	11.11	9.09
NKG2C	**7**	10.26	19.64	11.27	12.5	12.07	22.06	100	90.04	9.49	21.55	8.26	11.21	16.28	17.92	17.92	15.09	19.81	17.92
NKG2E	**8**	15.19	21.05	11.27	12.33	12.07	22.33	90.04	100	8.76	21.16	6.36	11.21	14.73	16.98	16.98	14.15	18.87	16.98
Common γc	**9**	17.24	10.59	13.79	13.57	13.53	15	9.49	8.76	100	22.22	8.43	11.45	9.85	14.75	13.11	13.66	14.21	13.11
IL2Rβ	**10**	21.57	14.65	18.09	12.86	12.5	15.12	21.55	21.16	22.22	100	17.52	18.35	13.28	13.27	14.29	14.29	13.27	13.78
CD2	**11**	10.85	10.45	8.46	9.62	10.16	13.21	8.26	6.36	8.43	17.52	100	18.63	19.07	19.68	20.74	20.21	18.62	19.68
CD16A	**12**	17.69	13.48	9.76	11.58	11.81	10.58	11.21	11.21	11.45	18.35	18.63	100	21.2	19.62	19.14	20.1	20.1	21.53
NCR1	**13**	14.29	15.13	6.57	10.28	12.59	13.6	16.28	14.73	9.85	13.28	19.07	21.2	100	34.76	34.76	34.33	33.91	33.48
KIR2DS4	**14**	12.82	13.73	8.45	12.38	10.42	11.11	17.92	16.98	14.75	13.27	19.68	19.62	34.76	100	89.39	90.2	86.53	86.94
KIR2DS1	**15**	12.82	13.73	7.75	13.33	13.19	10.1	17.92	16.98	13.11	14.29	20.74	19.14	34.76	89.39	100	92.65	91.43	92.24
KIR2DS2	**16**	12.82	13.73	9.15	13.33	11.11	11.11	15.09	14.15	13.66	14.29	20.21	20.1	34.33	90.2	92.65	100	91.84	91.43
KIR2DS3	**17**	11.97	14.38	8.45	15.24	11.81	11.11	19.81	18.87	14.21	13.27	18.62	20.1	33.91	86.53	91.43	91.84	100	92.65
KIR2DS5	**18**	11.97	13.73	8.45	13.33	11.81	9.09	17.92	16.98	13.11	13.78	19.68	21.53	33.48	86.94	92.24	91.43	92.65	100

ISSN 2616-0684 (Print)
ISSN 2616-0692 (Electronic)

Table 14: Summary of Receptor - Ligand Interactions and RMSF

S/N	Receptor	Total No. of interacting residues	Compounds with highest No. of bonds	Total No. of bonds	Types of bonds	Total RMSF
1	KIR2DS1	14	4'-Methyl-epigallocatechin	9	2	1.62
			Gibberellin A29	8	3	3.63
			Gibberellin A20	7	3	33.92
2	KIR2DS2	19	Gibberellin A51	10	3	18.65
			Monocrotalline	8	3	34.07
			Gibberellin A44	8	2	27.68
3	KIR2DS2	13	4'-Methyl-epigallocatechin	9	2	15.19
			Gibberellin A17	8	3	43.98
			Gibberellin A20	7	3	22.02
			Gibberellin A29	7	3	51.13
4	KIR2DS4	17	Gibberellin A51	8	2	1.47
			4'-Methyl-epigallocatechin	7	2	9.26
			Gibberellin A29	7	2	21.32
			Andrographis Extract	7	2	3.47
5	KIR2DS5	16	Andrographis Extract	10	3	19.16
			Gibberellin A44	9	2	4.8
			Gibberellin A17	5	3	8.29
6	NCR1	11	Gibberellin A51	10	3	46.9
			Gibberellin A19	10	2	20.36
			Gibberellin A44	8	3	29.58
7	NCR2	5	4'-Methyl-epigallocatechin	6	2	15.76
8	NCR3	12	Gibberellin A51	9	3	1.03
			Gibberellin A29	6	3	9.46
			Gibberellin A20	6	2	6.67
9	PILR	26	Eugenyl Glucoside	12	3	0.5
			4'-Methyl-epigallocatechin	11	2	1.34
			Andrographis Extract	10	2	7.78
10	CD16	6	Gibberellin A29	10	2	1.56
			Gibberellin A20	9	2	9.2
			Gibberellin A44	8	2	17.02
11	CD2	6	4'-Methyl-epigallocatechin	9	2	3.1
12	NKG2-C	4	Gibberellin A51	5	2	16.25
13	NKG2-D	32	4'-Methyl-epigallocatechin	11	2	6.55
			Gibberellin A17	10	3	7.13
			Gibberellin A51	9	3	13.15
			Gibberellin A19	9	3	36.43
14	NKG2-E	22	4'-Methyl-epigallocatechin	8	2	29.72
			Betulabuside A	8	2	14.12
			Shikimic acid	6	2	37.47
15	IL2Rα	8	4'-Methyl-epigallocatechin	9	2	4.83
			Monocrotalline	7	2	0.13
16	IL2Rβ	4	4'-Methyl-epigallocatechin	6	2	8.04
17	IL2Rγ	13	Gibberellin A29	11	3	11.79
			4'-Methyl-epigallocatechin	9	3	1.78

ISSN 2616-0684 (Print)
ISSN 2616-0692 (Electronic)

			Gibberellin A44	9	2	2.38
18	IL15Rα	3	4'-Methyl-epigallocatechin	3	2	14.38

The best 3 (or 4) receptor - ligand Interactions were selected as candidates for Normal Mode Analysis.

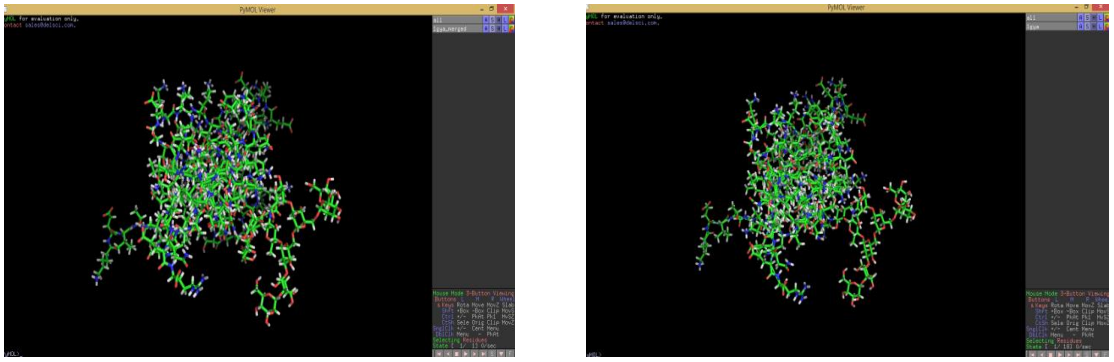

A **B**

Figure 2: Separated, docked and superimposed structure of 1gya as compared to the original structure. (A) Separated, docked & superimposed structure of 1gya. (B) Original Structure of 1gya

Conclusion

With the aim of triggering cytotoxicity, 1,697 natural compounds derived from 79 plants were docked against 18 activating NKC receptor targets. After rigorous screening, 17 bioactive, non-promiscuous hit compounds with good physicochemical and pharmacokinetic properties were identified.

To add value to the drug discovery process, lead optimization may be necessary to adjust the structures of the compounds to achieve stronger binding affinity, greater potency, and better ADMET-prediction. The identification of the pharmacophores of strong binding affinity-compounds, and the modification of their core structural moieties, could achieve the ideal pharmacokinetic properties.

A further molecular dynamics simulation study is required to confirm the viability of the 18 drug targets. With the right parameterization, the strength and sustainability of the molecular interactions between these proteins and the lead compounds will be predicted.

Conflict of interest

The authors declare no conflict of interest.

Authors' Declaration

The authors hereby declare that the work presented in this article is original and that any liability for claims relating to the content of this article will be borne by them.

Acknowledgements

The authors acknowledge the management of National Biotechnology Development Agency, Abuja, Nigeria for providing an enabling environment for this research work.

References

1. Margret CR, Prabakaran M, Jaykar B, Venkateswarlu B, Palanisamy P. BRCA mutation: A review of breast cancer. J Drug Disc Ther. 2019; 9(2-s):617-624.
2. WHO. "Cancer Fact Sheet N 297". World Health Organization. February 2018. Retrieved 21 March 2018.
3. Global, regional and national life expectancy, all-cause mortality, and cause-specific mortality for 249 causes of death, 1980–2015: a systematic analysis for the Global Burden of Disease Study 2015. Lancet. 2016; 388(10053): 1459-1544.
4. Poetsch AR, Boulton SJ, Luscombe NM. Genomic landscape of oxidative DNA damage and repair reveals regioselective protection from mutagenesis. Genome Biol. 2018; 19:215.
5. Jefford C and Irminger-Finger I. Mechanisms of chromosome instability in cancers. Crit Rev Oncol Hematol. 2006; 59:1-14.
6. Howarth K, Blood K, Ng B, Beavis J, Chua Y, Cooke S. Chromosome translocations in breast cancer. Breast Cancer Res. 2008; 10(2):6.
7. Idowu MO and Powers CN. Lung cancer cytology: potential pitfalls and mimics - a review. Int J Clin Exp Pathol. 2010; 3(4):367-385.
8. Beatty LG and Whitney LG. Immune escape mechanisms as a guide for cancer immunotherapy. Clin Cancer Res. 2015; 21(4):687-692.
9. Rowaiye AB, Asala T, Oli AN, Uzochukwu IC, Akpa A, Esimone CO. The Activating Receptors of Natural Killer Cells and Their Inter-Switching Potentials. Curr Drug Targets. 2020; 21(16): 1733-1751.
10. Rigsby RE and Parker AB. Using the PyMOL application to reinforce visual understanding of protein structure. Biochem and Molecular Bio Education. 2016; 44(5):433-437.
11. Waterhouse A, Bertoni M, Bienert S, Studer G, Tauriello G, Gumienny R. SWISS-MODEL: homology modelling of protein structures and complexes. Nucl Acids Res. 2018; 46(1):296-303.
12. Williams CJ, Headd JJ, Moriarty NW, Prisant MG, Videau LL, Deis LN, Verma V, Keedy DA, Hintze BJ, Chen VB, Jain S, Lewis SM, Arendall III WB, Snoeyink J, Adams PD, Lovell SC, Richardson JS, Richardson DC. MolProbity: More and better reference data for improved all-atom structure validation. Protein Sci. 2017; 27(1):293-315.
13. Ramachandran S, Kota P, Ding F, Dokholyan NV. Automated minimization of steric clashes in protein structures. Proteins. 2011; 79(1):261-270.

14. Dallakyan S and Olson AJ. Small-Molecule Library Screening by Docking with PyRx. Methods Mol Biol. 2015; 1263:243-250.
15. Kim S, Thiessen P, Bolton E, Chen J, Fu G, Gindulyte A, Han L, He J, He S, Shoemaker B, Wang J, Yu B, Zhang J, Bryant S. PubChem Substance and Compound databases. Nucl Acids Res. 2016; 44(D1):D1202-D1213.
16. Daina A, Michielin O, Zoete V. SwissADME: a free web tool to evaluate pharmacokinetics, drug-likeness and medicinal chemistry friendliness of small molecules. Sci Rep. 2017; 7:42717.
17. Backman TW, Cao Y, Girke T. ChemMine tools: an online service for analyzing and clustering small molecules. Nucl Acids Res. 2011; 39:W486-91.
18. Sievers F and Higgins DG. Clustal Omega for making accurate alignments of many protein sequences. Protein Sci. 2018; 27(1):135-145.
19. Salentin S. PLIP: fully automated protein-ligand interaction profiler. Nucl Acids Res. 2015; 43(W1):W443-W447.
20. Kuriata A, Aleksandra M, Gierut T, Oleniecki MP, Ciemny A, Kolinski M, Kurcinski SK. CABS-flex 2.0: a web server for fast simulations of flexibility of protein structures. Nucl Acids Res. 2018; 46(W1):W338-W343.
21. Xiang Z. Advances in homology protein structure modeling. Curr Prot Pept Sci. 2006; 7(3):217-227.
22. Ginalski K. Comparative modeling for protein structure prediction. Curr Opin Struct Biol. 2006; 16(2):172-177.
23. Das D, and Mukhopadhyay S. Studying backbone torsional dynamics of intrinsically disordered proteins using fluorescence depolarization kinetics. J Biosci. 2018; 43:455-462.
24. Chen B, Vincent W, Bryan AIII, Jeffrey JH, Daniel AK, Robert MI. MolProbity: all-atom structure validation for macromolecular crystallography. Acta Crystallogr D Biol Crystallogr. 2010; 66(1):12-21.
25. Subramani A and Floudas CA. Structure Prediction of Loops with Fixed and Flexible Stems. J Phys Chem B. 2012; 116(23):6670-6682.
26. Schneider M, Fu X, Keating AE. X-ray vs. NMR structures as templates for computational protein design. Proteins: Struct Funct Bioinform. 2009; 77(1):97-110.
27. Kushwah YS and Shrivastava RK. Energy minimization of protein structure using homology modeling and Particle Swarm Optimization with Dynamic Inertia Weights. IOSR J Comput Eng. 2017; 19(6):24-31
28. Shivanika C, Deepak KS, Venkataraghavan R, Pawan T, Sumitha A, Brindha DP. Molecular docking, validation, dynamics simulations, and pharmacokinetic prediction of natural compounds against the SARS-CoV-2 main-protease. J Biomol Structure Dynam. 2020 (Sept 8): 1–27.
29. Morak-Młodawska B, Pluta K, Jele M. Evaluation of the Lipophilicity of New Anticancer 1,2,3-Triazole-Dipyridothiazine Hybrids Using RP TLC and Different Computational Methods. Processes 2020; 8(7):858.
30. Isa MA, Mustapha A, Qazi S, Raza K, Allamin IA, Ibrahim MM & Mohammed MM. In silico molecular docking and molecular dynamic simulation of potential inhibitors of 3C-like main proteinase (3CLpro) from severe acute respiratory syndrome coronavirus-2 (SARS-CoV-2) using selected African medicinal plants. Adv Trad Med. 2020 (Nov 19): 1–17.
31. Zhang MQ and Wilkinson B. Drug discovery beyond the 'rule-of-five'. Curr Opin Biotechnol. 2007; 18(6):478-88.
32. Ganesan A. The impact of natural products upon modern drug discovery. Curr Opin Chem Biol. 2008; 12(3):306-317.
33. Paricharak S, Méndez-Lucio O, Ravindranath AC, Bender A, IJzerman AP, van Westen GJP (2018. Data-driven approaches used for compound library design, hit triage and bioactivity modeling in high-throughput screening. Briefings in Bioinformat. 2018; 19(2):277-285.
34. Hopkins AL. Pharmacological Space in the Practice of Medicinal Chemistry. (4th ed.). Pages 395-408.USA: Elsevier; 2015.
35. Zingoni A, Molfetta R, Fionda C, Soriani A, Paolini R, Marco Cippitelli, Cristina Cerboni and Angela Santoni. NKG2D and Its Ligands: "One for All, All for One". Front Immunol. 2018; 9: 476.
36. Vlieg HC, Huizinga EG, Janssen BJC. Structure and flexibility of the extracellular region of the PirB receptor. J Biol Chem. 2019; 294:4634-4643.
37. Schnell DJ. The TOC GTPase Receptors: Regulators of the Fidelity, Specificity and Substrate Profiles of the General Protein Import Machinery of Chloroplasts. Protein J. 2019; 38:343-350.
38. James SS and Michael JW. Practical application of ligand efficiency metrics in lead optimization. Bioorg Med Chem. 2018; 26(11):3006-3015.
39. Zhu T, Shuyi C, Pin-Chih S, Ram Patel, Darshan S, Heta BC. Hit Identification and Optimization in Virtual Screening: Practical Recommendations Based Upon a Critical Literature Analysis. J Med Chem. 2013; 56(17):6560-6572.
40. Kenny PW. The nature of ligand efficiency. J Cheminform. 2019; 11:8.
41. Von Korff M and Sander T. Molecular Complexity Calculated by Fractal Dimension. Sci Rep. 2019; 9:967.
42. Feldmann C, Miljković F, Yonchev D, and Bajorath J. Identifying Promiscuous Compounds with Activity against Different Target Classes. Molecules. 2019; 24(22):4185.
43. Dhillon B, Narendra KG, Rishabha M, Pramod KS. Poorly Water-Soluble Drugs: Change in Solubility for Improved Dissolution Characteristics - A Review. Glob J Pharmacol. 2014; 8(1):26-35.
44. Szisz D and Antal L. Solubility prediction - ChemAxon's Solubility Predictor. [Online]. 2018. Available from: https://chemaxon.com/news/solubility-prediction-chemaxons-solubility-predictor. Accessed on the 4th of April, 2020
45. Van-Breemen RB and Li Y. Caco-2 cell permeability assays to measure drug absorption. Expert Opin Drug Metab Toxicol. 2005; 1(2):175-185.
46. Basant N, Gupta S, Singh KP. Predicting human intestinal absorption of diverse chemicals using ensemble learning based QSAR modeling approaches. Comput Biol Chem. 2016; 61:178-196.
47. Faralli A, Shekarforoush E, Ajalloueian F, Mendes AC, Chronakis IS. *In vitro* permeability enhancement of curcumin across Caco-2 cells monolayers using electrospun xanthan-chitosan nanofibers. Carbohydr Polym. 2019; 15(206):38-47.
48. Waghray D and Zhang Q. Inhibit or Evade Multidrug Resistance P-glycoprotein in Cancer Treatment. J Med Chem. 2018; 61(12):5108-5121.
49. Han Y, Zhang J, Hu CQ, Zhang X, Ma B, Zhang P. *In silico* ADME and Toxicity Prediction of Ceftazidime and Its Impurities. Front Pharmacol. 2019; 10:434.
50. Lewis DF. Human cytochromes P450 associated with the phase 1 metabolism of drugs and other xenobiotics: a compilation of substrates and inhibitors of the CYP1, CYP2 and CYP3 families. Curr Med Chem. 2003; 10:1955-1972.
51. Stavropoulou E, Pircalabioru GG, Bezirtzoglou E. The Role of Cytochromes P450 in Infection. Front Immunol. 2018; 9:89.
52. Pires DEV, Blundell TL, Ascher DB. pkCSM: predicting small-molecule pharmacokinetic properties using graph-based signatures. Journal of Medicinal Chemistry. 2015; 58 (9): 4066–4072.
53. Hu J, Webster D, Cao J, Shao A. The safety of green tea and green tea extract consumption in adults – Results of a systematic review. Regulatory Toxicology and Pharmacology. 2018; 95:412-433.

54. Khan T, Shalini D, Rumana A, Saman R, Iqbal A, Seema J, Abdul RK. Molecular docking, PASS analysis, bioactivity score prediction, synthesis, characterization and biological activity evaluation of a functionalized 2-butanone thiosemicarbazone ligand and its complexes. J Chem Biol. 2017; 10(3):91-104.
55. Eaton BE, Gold L, Zchi DA. Let's get specific: the relationship between specificity and affinity. Chem Biol. 1995; 2(10):633-638.
56. Guo ZR. Drug promiscuity. Yao Xue Xue Bao. 2011; 46(4):361-369.
57. Tanford C. Chemical basis for antibody diversity and specificity. Accounts of Chem Res. 1968; 1(6):161-167.
58. Kubinyi H. Chemical Similarity and Biological Activities. J Braz Chem Soc. 2002; 13(6):717-726.
59. Che J, Wang Z, Sheng H, Huang F, Dong X, Hu Y, Xie X, Hu Y. Ligand-based pharmacophore model for the discovery of novel CXCR2 antagonists as anti-cancer metastatic agents. R Soc Open Sci. 2018; 5:180176.
60. Croce G, Gueudré T, Ruiz Cuevas MV, Keidel V, Figliuzzi M, Szurmant H, Weigt M. A multi-scale coevolutionary approach to predict interactions between protein domains. PLoS Comput Biol. 2019; 15(10):e1006891.
61. Wang Y, Wu H, Cai Y. A benchmark study of sequence alignment methods for protein clustering BMC Bioinformatics. 2018; 19(19):529.
62. Stauber DJ, Debler EW, Horton PA, Smith KA, Wilson IA. Crystal structure of the IL-2 signaling complex: paradigm for a heterotrimeric cytokine receptor. Proc Natl Acad Sci. 2006; 103(8):2788-2793.
63. Güldenhaupt J, Amaral M, Kötting C, JSchartner J, Musil D, Frech M, and Gerwert K. Ligand-Induced Conformational Changes in HSP90 Monitored Time Resolved and Label Free—Towards a Conformational Activity Screening for Drug Discovery. Angew Chem Int Ed Engl. 2018; 57(31):9955-9960.
64. Mishra SK, Tripathi S, Shukla A, Oh SH, Kim HM. Andrographolide and analogues in cancer prevention (Elite Ed). Front Biosci. 2015; 7:255-266.
65. Puri A, Saxena R, Saxena RP, Saxena KC, Srivastava V, Tandon JS. Immunostimulant agents from *Andrographis paniculata*. J Nat Prod. 1993; 56(7):995-999.
66. Sheeja K and Kuttan G. Modulation of natural killer cell activity, antibody-dependent cellular cytotoxicity, and antibody-dependent complement-mediated cytotoxicity by andrographolide in normal and Ehrlich ascites carcinoma-bearing mice. Integr Cancer Ther. 2007; 6(1):66-73.
67. Sheeja K and Kuttan G. *Andrographis paniculata* downregulates proinflammatory cytokine production and augments cell mediated immune response in metastatic tumor-bearing mice. Asian Pac J Cancer Prev. 2010; 11(3):723-729.
68. Asami T and Nakagawa Y. Brief review of plant hormones and their utilization in agriculture. J Pest Sci. 2018; 43(3):154-158.
69. Koshioka MT and Nishijima HY. Endogenous gibberellins in the immature seeds of okra (*Abelmoschus esculentus*). J Plant Physiol. 1996:149(1–2):129-132.
70. Yu-xian Z, Davies PJ, Halinska A. Metabolism of Gibberellin A12 and A12-Aldehyde in Developing Seeds of *Pisum sativum* L. Plant Physiol. 1991; 97:26-33.
71. Scha¨fer P, Stefanie P1, Lars M, Doreen Z, Peter M, Chandler FW. Karl-Heinz K. Manipulation of plant innate immunity and gibberellin as factor of compatibility in the mutualistic association of barley roots with *Piriformospora indica*. The Plant J. 2009; 59:461-474.
72. Vidhyasekaran P. Plant Hormone Signaling Systems in Plant Innate Immunity. Part of the Signaling and Communication in Plants book series. SIGCOMM. 2014; 2:383-401.
73. Zhang Y, Hui Z, Jingbo C, Haixia Z, Xianghui Z, Hongbin Z, Chen Q. Antitumor and antiangiogenic effects of GA-13315, a gibberellin derivative. Investig New Drugs. 2012; 30(1):8-16.
74. Shen S and Tang J. Effects and mechanism of GA-13315 on the proliferation and apoptosis of KB cells in oral cancer. Oncol. Letters 2017; 14(2):1460-1463.
75. Mo J, Kang M, Ye JX, Chen JB, Zhang HB, Qing C. Gibberellin derivative GA-13315 sensitizes multidrug-resistant cancer cells by antagonizing ABCB1 while agonizes ABCC1. Cancer Chemother Pharmacol. 2016; 78(1):51-61.
76. Chen J, Sun Z, Zhang Y, Zeng X, Qing C, Liu J, Li L, Zhang H. Synthesis of gibberellin derivatives with anti-tumor bioactivities. Bioorg Med Chem Lett. 2009; 19(18):5496-5499.
77. Murata T, Fushinobu S, Nakajima M, Asami O, Sassa T, Wakagi T, Yamaguchi SI. Crystal structure of the liganded anti-gibberellin A (4) antibody 4-B8(8)/E9 Fab fragment. Biochem Biophys Res Commun. 2002; 293(1):489-496.
78. Tringali C, Carmela S, Onofrio DL. Bioactive constituents of the bark of *Parkia biglobosa.* Fitoterapia. 2000; 71(2):118-125.
79. Yashi AY, Boris VN, Emilie C, Yakov IY. Determination of the Chemical Composition of Tea by Chromatographic Methods: A Review. J Food Res. 2015; 4(3): 56-88.
80. Khan N and Mukhtar H. Multitargeted Therapy of Cancer by Green Tea Polyphenols. Cancer Lett. 2008; 269(2):269-280.
81. Orentas RJ. Reading the tea leaves of tumor-mediated immunosuppression. Clin Cancer Res. 2013; 19(5):955-957.
82. So-Youn M, Mei Y, Sang BK, Sneha R, Seong-Ryuel K, Kamala V, Ho-Youn K, Laurie SD. Green Tea Epigallocatechin-3-Gallate Suppresses Autoimmune Arthritis Through Indoleamine-2,3-Dioxygenase Expressing Dendritic Cells and the Nuclear Factor, Erythroid 2-Like 2 Antioxidant Pathway. J Inflamm. 2015; 12:53.
83. Chen X, Li X, Zhai X, Zhi X, Cao L, Qin L, Su J. Shikimic Acid Inhibits Osteoclastogenesis *in Vivo* and *in Vitro* by Blocking RANK/TRAF6 Association and Suppressing NF-κB and MAPK Signaling Pathways. Cell Physiol Biochem. 2018; 51:2858-2871.
84. Lima LGB, Montenegro J, de Abreu JP, Santos MCB, do Nascimento TP, Santos MD, Ferreira AG, Cameron LC, Ferreira MSL and Teodoro AJ. Metabolite Profiling by UPLC-MSE, NMR, and Antioxidant Properties of Amazonian Fruits: Mamey Apple (*Mammea americana*), Camapu (*Physalis angulata*), and Uxi (*Endopleura uchi*). Molecules 2020; 25:342.
85. Farrell N, Roberts JD, Hacker MP. Shikimic acid complexes of platinum. Preparation, reactivity, and antitumor activity of (R,R-1,2-diaminocyclohexane) bis(shikimate) platinum (II). Evidence for a novel rearrangement involving platinum-carbon bond formation. J Inorg Biochem. 1991; 42(4):237-246.
86. Zhang Y, Liu A, Ye ZG, Lin J, Xu LZ, Yang SL. New approach to the total synthesis of (-)-zeylenone from shikimic acid. Chem Pharm Bull. 2006; 54:1459.
87. Sánchez-Abella L, Fernández S, Armesto N, Ferrero M, Gotor V. Novel and efficient syntheses of (-)-methyl 4-epi-shikimate and 4,5-epoxyquinic and -shikimic acid derivatives as key precursors to prepare new analogues. J Org Chem. 2006; 71(14):5396-5399.